Measuring Drop-Size Distributions in Clouds with a Clear-Air-Sensing Doppler Radar

EARL E. GOSSARD

Cooperative Institute for Research in the Environmental Sciences (CIRES), University of Colorado/NOAA, Boulder, Colorado

(Manuscript received 7 December 1987, in final form 17 February 1988)

ABSTRACT

The advent of Doppler clear-air radars for wind-height profiling opens the way for their use in a variety of other applications. This paper uses knowledge of the clear-air Doppler spectrum from a zenith-pointing radar together with the measured water droplet Doppler vertical velocity spectrum to calculate spectra of drop number density through clouds of droplets having substantial fall velocity. The method has been applied by Japanese scientists to measure drop-size distributions of precipitation particles from data acquired at the VHF MU radar facility. Here the method is applied to records obtained with a 915 MHz wind profiler located at Denver, Colorado, and the resulting spectra are presented and compared with the spectra that would have been obtained if the clear-air information were ignored. From the number density drop-size distribution, the corresponding liquid water distribution can be calculated. It is concluded that failure to take into account turbulence in the medium can result in order-of-magnitude errors in number density and liquid water. The requirements and limitations of a radar remote sensing drop spectrometer are discussed.

1. Introduction

Because radar backscattered power depends on the size and number of drops in the pulse volume, one of the earliest uses of Doppler radars for meteorological purposes was an attempt to measure drop-size distributions by assuming that the Doppler velocity spectrum of a vertically pointing radar was a direct measure of the droplet fall velocity spectrum. The measured backscattered power spectrum versus vertical velocity (the Doppler spectrum) was then converted to backscattered power spectrum versus drop size by using some empirical or semiempirical size versus fall velocity (in quiet air) relationship. Experiments were carried out by many investigators; e.g., Boyenval (1960), Lhermitte (1960), Rogers and Pilié (1962), Wilson (1963), Caton (1963, 1966), du Toit (1967) and Gorelik et al. (1967). A complete discussion of the state of the methodology as of 1973 was given by Atlas et al. (1973) and, more recently, by Doviak and Zrnić (1984). The drop size versus fall velocity in quiet air is fairly well known (e.g., Gunn and Kinzer 1949; du Toit 1967; Foote and DuToit (1969); Ugai et al. 1977), so in quiet air the conversion of a measurement of the fall velocity spectrum to a drop-size spectrum is straightforward. Complications arise when the particles are not in quiet air, but are, in fact, embedded in a turbulent medium that may have a net updraft or downdraft. Until the advent of clear-air radars this complication was insurmountable, although as noted above, many experiments were done under conditions when the investigators believed atmospheric conditions to be relatively quiet. They neglected turbulence, and they used various methods to estimate the mean vertical wind. The accuracy of the estimated vertical wind was only about 1 m s^{-1} which was not accurate enough for determining the size distributions of the smaller particles (Atlas et al. 1973).

Wakasugi et al. (1986, 1987) pointed out that clear-air radar wind profilers provide the necessary information on clear-air structure (note spectral peak near $W = 0$ in Fig. 1) to allow the crucial corrections for a nonquiescent medium to be made, and Doppler radars should now be able to collect accurate spectra of drop number density and liquid water density remotely for a wide range of liquid water clouds using the water droplet return. The cloud return creates the spectral peak near $W = 1.2$ m s^{-1} at range gates above number 15 in Fig. 1. This pattern of abrupt change at cloud height and its temporal repeatability are important factors in separating the cloud return from that of the clear air.

2. Formulation of the problem

The total backscattered power is the sum of the return from the clear air and from the droplet population and is given by

$$P_r = CP_t \frac{\Delta r}{r^2} \eta \qquad (1)$$

where η is the radar reflectivity, C is $\pi A_e/[64\ (2\ln 2)]$ for an antenna of effective area A_e and Gaussian pattern, P_t is transmitted power, r is range, Δr is range resolution and λ is radar wavelength. If the power re-

Corresponding author address: Dr. Earl Gossard, NOAA, 325 Broadway, Boulder, CO 80303.

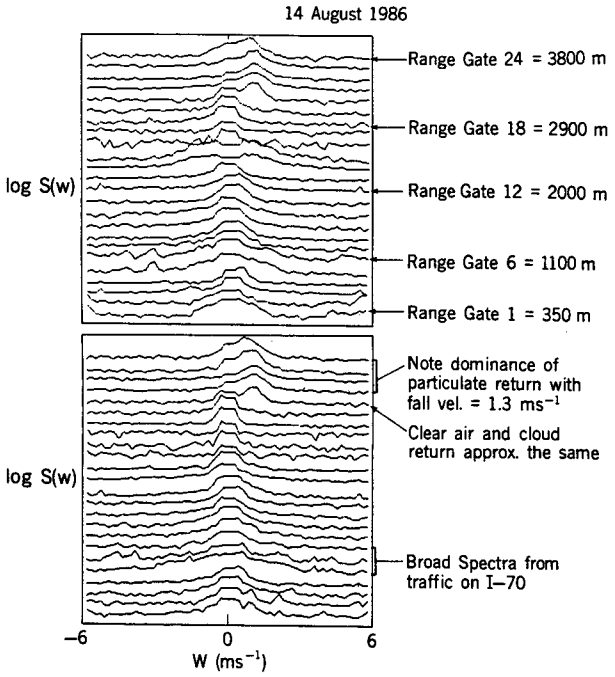

FIG. 1. Sample of two successive height sequences (upper and lower frames) of stacked Doppler spectra in each of 24 range gates from vertically pointing, 915 MHz radar recorded at 1212 MST (see virga in Fig. 5). The time separation of the sequences is 25 s. The spectra were obtained by 64 point FFTs with a velocity resolution of 0.18 m s^{-1}. Most spectra show only one main peak due to clear-air return centered near zero on the vertical velocity scale. Above the 19th range gate, a second peak centered on a velocity somewhat greater than 1 m s^{-1} is evident due to radar return from falling water droplets. The flat portion of the spectra at $W = 0$ is an artifact resulting from the removal of the spike due to stationary targets by interpolating across the zero velocity value.

turned from a droplet ensemble is represented by the "radar reflectivity factor" Z, the scatter from liquid water droplets is [e.g., Gossard and Strauch 1983, Eq. (2-31)]

$$\eta = 0.93(\pi^5/\lambda^4)Z \tag{2}$$

and the scatter from turbulent fluctuations of refractive index n in the clear air is [e.g., Gossard and Strauch 1983, Eq. (2.46)]

$$\eta = 0.38\lambda^{-1/3}C_n^2 \tag{3}$$

where C_n^2 is the structure parameter of the turbulent refractive index fluctuations when an inertial subrange of turbulence exists within which the scale $\lambda/2$ lies. Z is related to the number density and size of Rayleigh (small water droplet) scatterers as Z (mm^6 m^{-3}) $= \int_0^\infty N(D)D^6dD$ where $N(D)$ is the drop number density per cubic meter per unit D where D is drop diameter in mm. For simplicity, instead of using (3) we will treat the backscatter from the clear air as though it came from a droplet ensemble with an "equivalent" Z to be used in (2).

The complexity introduced by a nonquiescent medium effects the interpretation of the vertical velocity spectrum contributed by the droplet return. It is twofold: 1) An average upward or downward wind causes a mean shift in the measured Doppler velocity so that the spectrum would have a mean offset. 2) Turbulence causes drops of a given size to move upward or downward at different rates within the pulse volume. Thus a homogeneous population of droplets of the same size would provide a Doppler spectrum of substantial width, rather than a simple shifted spectral line.

Point 1 means that the mean vertical wind must be known to correct for the offset of the velocity axis of the spectrum.

Point 2 means that the spectral power associated with any given vertical velocity is composed of contributions from a range of drop sizes because within the same pulse volume drops of different sizes may have the same vertical velocity due to velocities superimposed by the turbulent medium.

Consider the case of a homogeneous distribution of drops, all with diameter D_1, with a quiet-air fall velocity of W_1. Assume no vertical wind and assume that the droplets instantaneously follow the turbulent fluctuations of the medium. Also assume the turbulent velocity distribution to be Gaussian (e.g., Batchelor 1959; Lumley and Panofsky 1964; Tennekes and Lumley 1972) with the clear-air backscatter spectrum S_c in equivalent Z units (Z_c) given by

$$S_c(W) = \frac{Z_c}{\sqrt{\pi W_\sigma^2}}\, e^{-(W/W_\sigma)^2}. \tag{4}$$

After subtracting the clear-air contribution from the total spectrum, only the water droplet contribution remains. The Doppler spectrum of backscattered power is Gaussian if the turbulent velocity distribution is Gaussian (e.g., Labbitt 1981) so, if the drops respond instantaneously to the medium, the Doppler spectrum due to drops of size D_1 is given by

$$S_1(W') = s_1(W_1)e^{-[(W'-W_1)/W_\sigma]^2} \tag{5}$$

where $s_1 = Z_1/\sqrt{\pi W_\sigma^2}$ and W_σ is the half-width of the Gaussian function at the e^{-1} point (instead of the $e^{-1/2}$ point often used). The situation is shown schematically in Fig. 2, where W_1 is the fall velocity of drops D_1 in quiet air and ΔW is the velocity resolution from the spectral analysis; W' represents the actual vertical velocity of the drops and is the velocity over which the integration of the function will be carried out from $-\infty$ to $+\infty$ to find the total power from drops of size D_1; and $s_1(W_1)$ is the spectral density from drops of size D_1 moving at the quiet-air velocity $W' = W_1$; S_{Q_1} is the equivalent power spectral density that would have been measured in the absence of turbulence when all the backscatter would be in one velocity resolution increment, i.e., $Z_1 = S_{Q_1}\Delta W$.

The real distribution of drops is not homogeneous,

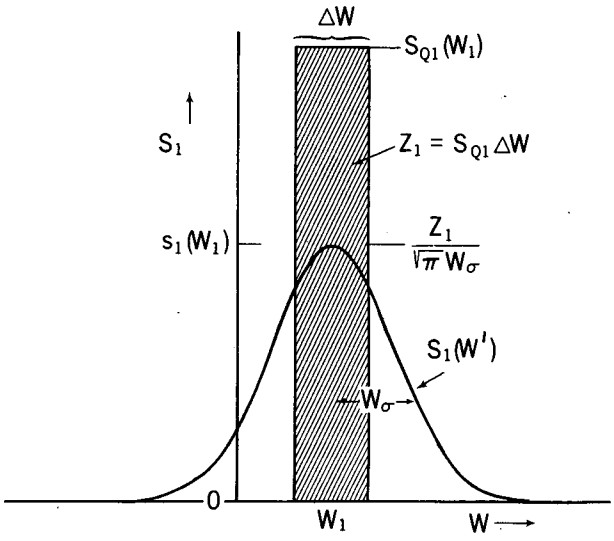

FIG. 2. Schematic illustration of the effect of a medium with Gaussian turbulence on the radar Doppler spectrum from a population of spherical water drops of uniform size with quiet-air terminal velocity of W_1. Hashed area represents the spectrum in still air for the velocity resolution interval ΔW centered on W_1. The Gaussian curve represents the corresponding spectrum smeared by Gaussian turbulence. S_{Q_1} is the power density that would have been found in the absence of turbulence when the return is all concentrated in a single velocity interval ΔW. Then the hashed area $Z_1 = S_{Q_1}\Delta W$ where Z_1 is the increment of Z centered on W_1.

with diameter D_1, but is a continuum so that, generalizing, the integral

$$S(W)\Delta W = \int_{-\infty}^{\infty} s(W')e^{-(W'-W/W_\sigma)^2}dW' \quad (6)$$

gives the total backscattered power contributed to ΔW by drops of all sizes with quiet-air fall velocity of W. Noting the relationship between s and S_Q defined in Fig. 2, this integral can be written as the convolution, $S_Q(W)*S_c(W)/Z_c$, and is equivalent to the droplet part of Eq. (1) of Wakasugi et al. (1987). (Wakasugi et al. use a normalized form of the Doppler spectrum equal to ours divided by Z.) The problem is, therefore, the deconvolution of Eq. (6) to find $S_Q(W)$ from the radar-measured value of $S(W)$. Like us, Wakasugi et al. (1987) choose the Gaussian form for the clear-air spectrum (e.g., Labbitt 1981). In addition, they choose an exponential form for the drop-size spectrum and carry out a least-squares best fit of the exponential form to their measurements. In this paper the deconvolution is treated as a mathematical inversion problem and an elementary retrieval method is used to obtain the cloud drop-size distribution. Such a method contains the usual hazards of potential ambiguity in the solution, but if the drop-size distribution has a relatively simple form, the results should be accurate. It has the advantage of not being restricted to a single functional form, and in the present examples the spectral distribution has been extended to the small droplet part of the spectrum where number density may even increase with drop size. The accuracy of the estimate of course diminishes toward the small drop-size end of the distribution because the fundamental information on size is the measured fall velocity. As the fall velocity becomes smaller relative to W_σ, longer and longer averages are required to obtain a reliable fall velocity estimate.

To obtain a first estimate of $s(W)$, we assume it to be a linear function in the neighborhood of W (essentially over a band of width W_σ) and carry out the integration over W' indicated in (6) to obtain the local analytical relationship between $s(W)$ and $S(W)$. From the radar measurement of $S(W)$, a value of $s(W)$ is found and inserted into (6); then the integration is carried out numerically over all W'. If W_σ is fairly large, it is found that the resulting calculated spectrum $S(W)$ is broader than the radar-measured spectrum and is reduced in amplitude at the maximum. Therefore an empirical shaping factor

$$\frac{A}{\left[1+\left(\frac{W-W_M}{W_0}\right)^2\right]^n} \quad (7)$$

was used to obtain an improved second estimate where W_M is the velocity at the maximum of the spectrum. After suitable trial-and-error adjustment of the constants A, W_0 and n, the factor (7) yielded good agreement with the measured $S(W)$ (Fig. 3, top frame). Clearly, more refined retrieval methods are possible and are under development. The quantity $s(W)$ is the spectral distribution (envelope) of Z associated with those drops that are falling with the most probable velocity, which we assume to be the quiet-air fall velocity after the mean up- or downdraft (found from the displacement of the clear-air peak from zero) has been removed. The sum of contributions from all W' is then contracted to the velocity interval centered on W as shown in Fig. 2 to obtain the equivalent spectral value, S_Q, that would have applied if the drops of each size had all been concentrated in the increment ΔW associated with the appropriate velocity in quiet air (rather than spread over W' as in a turbulent medium). An example (gate 16) is shown in the top frame of Fig. 3 in which original measured values of $S(W)$ (in Z units) are shown along with the final retrieved estimate of $S(W)$, found after integrating (6), and the equivalent spectrum for quiet air, $S_Q(W)$. The bottom frame of Fig. 3 shows the Gaussian distribution, determined from the clear-air portion of the Doppler spectrum, used to obtain the value of W_σ needed in the retrieval process. The spectrum S_Q for quiet air is designated as $S_Q(W)$ or $S_Q(D)$ according to whether the spectrum applies to vertical velocity or to drop size.

Having chosen radar reflectivity factor Z to represent the power [$S_Q(W) = \Delta Z/\Delta W$ in the spectral analysis], these spectra can immediately be expressed in terms

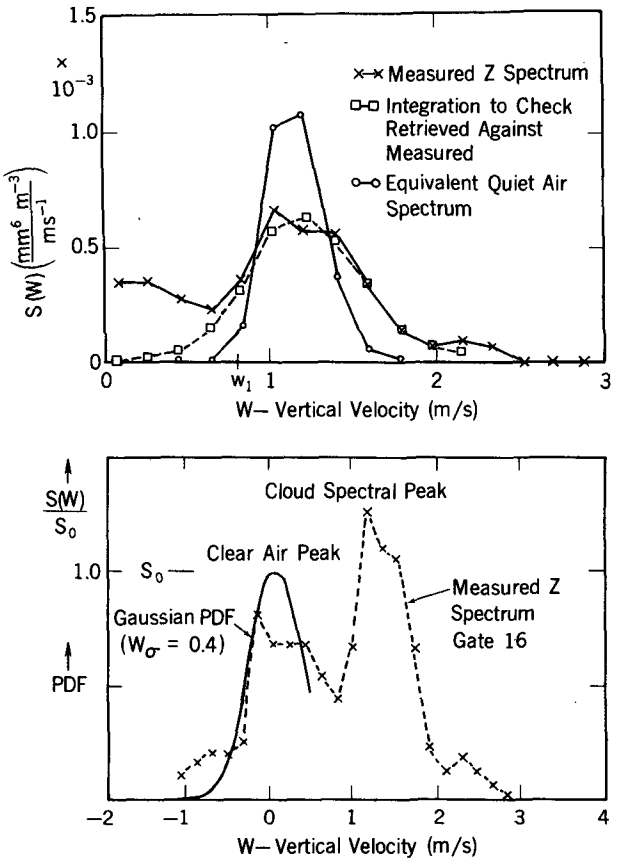

FIG. 3. Illustration of method of this paper using the measured spectrum from gate 16 at 1241 MST as an example. Top frame: Points indicated by x are observed spectra of contribution of all drops. After integration of contribution from all drops, the points indicated by squares are found, and the curve joining these points should agree well with the observed points (x) if the retrieved values have been correctly found. The relatively large values near $W = 0$ are, of course, due to clear-air return and are near zero after subtraction of the clear-air spectral points. Finally the contraction of the retrieved spectrum yields the equivalent quiet-air spectrum we seek (the points indicated by circles). Bottom frame: Example of fitting a Gaussian function to the measured clear-air spectrum. The two measurements near $W = 0$ are artificial; they are interpolated across zero because of the strong clutter from stationary targets.

of number density $N(D)$; see e.g., Battan 1973; Atlas 1964; Gossard and Strauch 1983; Doviak and Zrnić 1984). That is,

$$\Delta Z = N(D)D^6\Delta D \tag{8}$$

where Δ refers to the incremental resolution of the FFT spectrum analysis. Defining quantities as shown in Fig. 2,

$$\Delta Z = S_Q(W)\Delta W$$

so that ΔZ (the shaded area) represents the received power [see Eq. (1)] in the increment ΔW. Then

$$N(D) = D^{-6}\frac{\Delta W}{\Delta D}S_Q(W) = D^{-6}S_Q(D) \tag{9}$$

where $S_Q(D) = \Delta Z/\Delta D = (\Delta W/\Delta D)S_Q(W)$. For the W versus D relationship, we use a numerical fit to the curve found by du Toit (1967), using data from Gunn and Kinzer (1949), for a pressure level of 800 mb. (Typical surface pressures at Denver are about 840 mb.) The numerical fit we choose for $W \leq 3$ m s^{-1} is

$$D \approx 0.122W + 0.0206W^2. \tag{10}$$

Figure 4 shows du Toit's curves and compares (10) with data collected by Ugai et al. (1977) at approximately sea level pressures. From Eq. (10),

$$\frac{dD}{dW} = 0.122 + 0.0412W$$

so that

$$S_Q(D) = \frac{S_Q(W)}{0.122 + 0.0412W}. \tag{11}$$

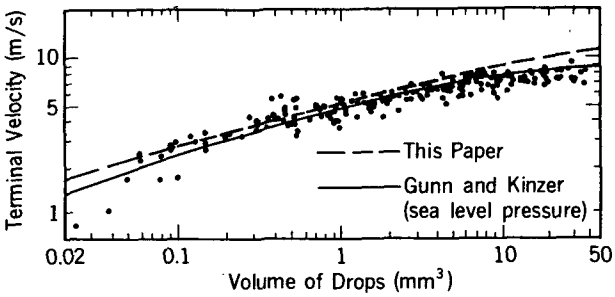

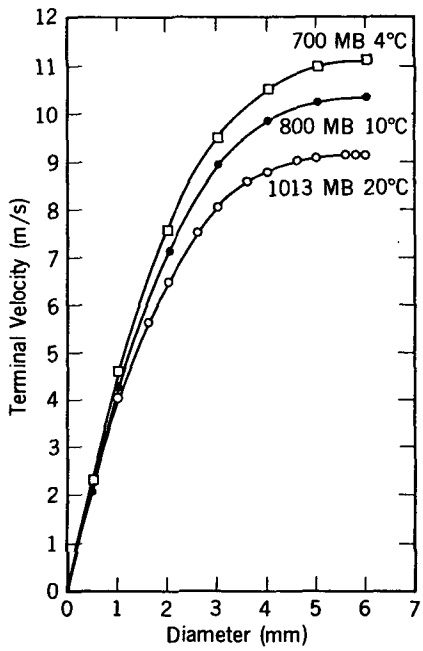

FIG. 4. The quiet-air terminal velocity of water drops vs drop size. Top frame: measurements by Ugai et al. (1977) compared with Gunn and Kinzer's (1949) result for sea level pressures and our Eq. (6) found by fitting a polynomial to the 800-mb curve of du Toit (1967) (bottom frame) for $W < 3$ m s^{-1}. For $D < 0.1$ mm, the Stokes relation fits the data better (Beard and Pruppacher, 1969).

The result can also be expressed in terms of a liquid water density spectrum [e.g., Eq. (4-5b) in Gossard and Strauch 1983]. If the mass density of liquid per cubic meter of air is M,

$$\Delta M(D) = \rho_L\left(\frac{\pi}{6}\right)N(D)D^3\Delta D$$

$$= \rho_L\left(\frac{\pi}{6}\right)D^{-3}\frac{\Delta W}{\Delta D}S_Q(W),$$

where ρ_L is density of liquid water (i.e., $\rho_L \approx 1$ g cm^{-3}). Then defining $S_M(D) = \Delta M/\Delta D$ and using (8) we find

$$S_M(D) = \rho_L\left(\frac{\pi}{6}\right)D^{-3}S_Q(D). \qquad (12)$$

3. The radar observations

The data analyzed in this paper were collected with a 915 MHz radar located at Stapleton Airport, Denver, Colorado. The radar system has been described by Strauch et al. (1984) and the data collection by Sengupta et al. (1987). Although the radar's primary use is profiling the horizontal winds, in the present study it was operated in a vertically pointing mode collecting a Doppler spectrum every 25 s. The radar characteristics are given in Table 1.

Figures 5 and 6 show an example of radar observations of a stratus cloud layer under conditions when there was no precipitation at the ground although the radar records clearly show virga below the cloud base.

TABLE 1. Radar characteristics.

Data processing information	
Pulse width	1 μs
Pulse repetition period	50 μs
Average power	110 W
Time domain averaging	136 pulses
Spectral averaging	11 spectra
Maximum radial velocity	±6 ms^{-1}
Spectral resolution (64 points)	0.188 m s^{-1}
Sample repetition period	24.5 s
Height sampling	
First height	350 m
Height spacing	150 m
Number of heights (gates)	24
Radar parameters	
Frequency	915 MHz
Maximum bandwidth	2 MHz
Peak power	5.6 kW
Duty cycle	<25%
Antenna aperture	100 m^2
Antenna type	Paraboloid with offset horn feeds
Two-way beamwidth	1.7°
System noise temperature	240 K

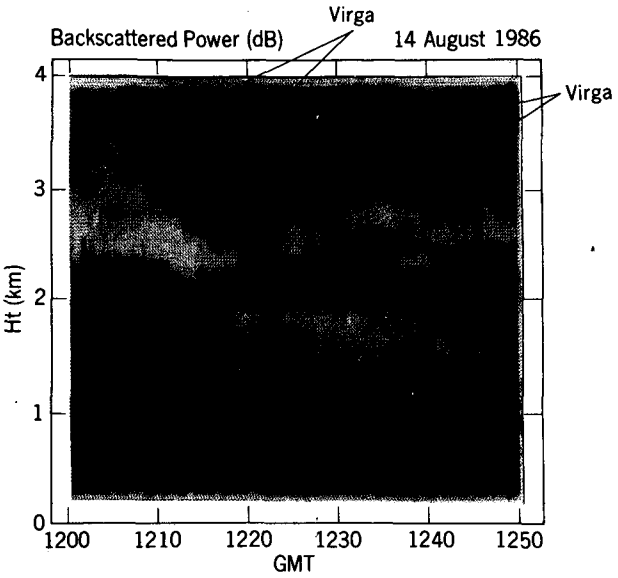

FIG. 5. Height–time plot of backscatter power intensity including time interval analyzed in this paper. Downward sloping streaks indicate virga with descent rates of about 1.3–1.5 m s^{-1} (see temperature sounding in Fig. 6).

Figure 7 shows examples of the power spectra analyzed in this paper at 1241:03 UTC when well-defined virga are seen in Figs. 5 and 6. This case was chosen because the surface-based, upward-looking microwave radiometer indicated the clouds to be liquid. The presence of liquid does not, alone, rule out the possible presence of graupel in the virga, but we also note the lack of any enhancement in radar reflectivity at the melting level (a bright band effect) in Fig. 5. We therefore conclude that the clouds are likely to be liquid.

The amplitude of the stacked spectra in Fig. 1 is scaled arbitrarily in the computer graphics, but an example of a quantitative spectrum (for gate 16) is shown in Fig. 3 where the ordinate scale is expressed in S (mm^6 m^{-3}/m s^{-1}). The total Z based on backscattered power for gate 16 is 0.5 mm^6 m^{-3}, or −28 dBZ. For gate 18 it is about an order of magnitude greater. The 1200 UTC radiosonde sounding information is superimposed on Fig. 6 and it defines clearly the height zone of the main stratus deck.

4. Data analysis

Gates 16, 17 and 18 were analyzed in detail since they represent a cross section of particle size information through the edge of liquid virga and into the interior. Furthermore, the analysis of these data provide examples of several important considerations when carrying out such an analysis.

At small drop size, the clear-air contribution may completely dominate the total contribution to the backscattered power as illustrated in Fig. 3.

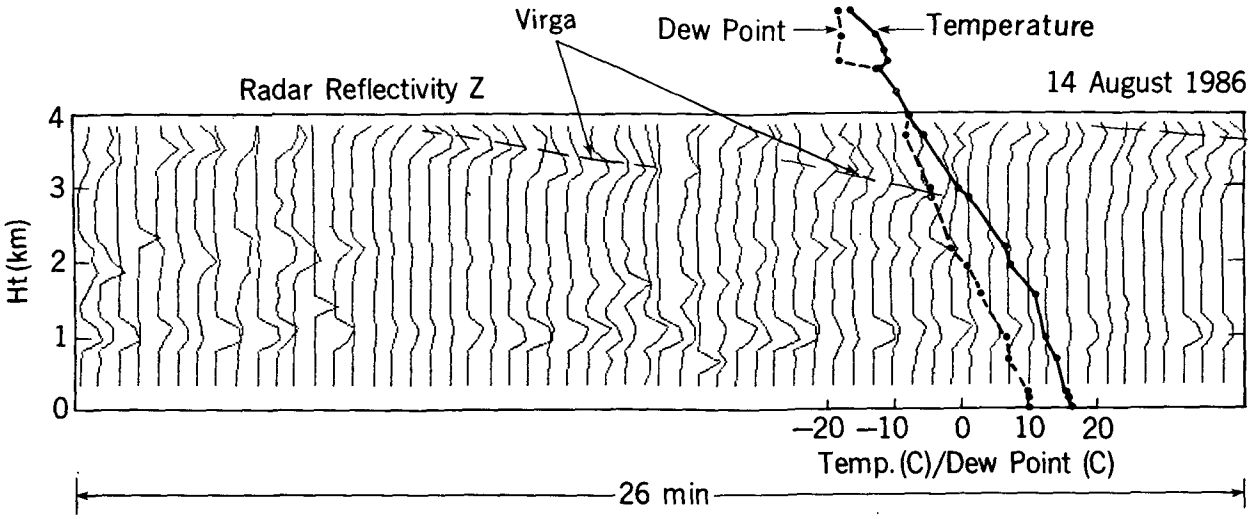

FIG. 6. Sample of same data as in Fig. 5 presented as side-by-side profiles of backscattered power vs height. Again, descending peaks indicate the virga analyzed in this paper.

a. Effect of turbulent spectral width

It is clear that the broadening effect of turbulence on the fall velocity spectrum is of the same order as the spread of the fall velocity itself for the droplets sensed in this experiment. It is therefore important to consider turbulence effects carefully in interpreting spectral form. We note from Fig. 3 that a choice of $W_\sigma = 0.4$ (m s^{-1}) for range gate 16 results in a good fit to the left-hand side of the clear-air peak of the spectrum,

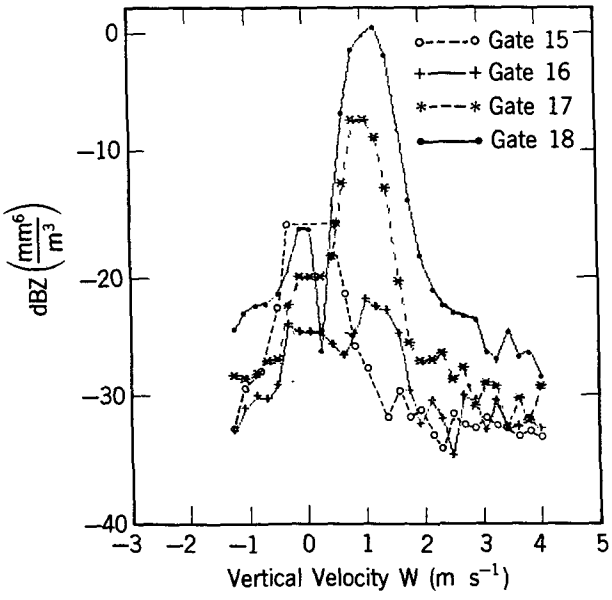

FIG. 7. Plot of backscatter (Z) spectra for gates 15, 16, 17 and 18 at 1241:03 on 14 August 1986. Gate 15, below the virga, shows no evidence of droplet backscatter but a very strong clear-air return. The flat portion at $W = 0$ is artificially produced by interpolation across zero to remove the spike due to clutter from stationary targets.

and the distributions of number density and liquid water for gate 16 were calculated with this assumption. Similar reasoning suggests a value of $W_\sigma = 0.3$ (m s^{-1}) for gates 17 and 18. From Fig. 7 we note that in all three range gates, the slope of the small droplet side of the spectrum is as steep or steeper than the large drop-size portion of the spectrum. (In gate 18 the slopes are about the same.) This means that the movement of the smallest droplets is dominated by turbulence and that the slope of the droplet spectrum on the small drop side of the spectral peak may be used as a measure of the clear-air spectral width when the clear-air return is submerged beneath the droplet return.

5. Results and discussion

Figures 8 and 9 show the calculated distributions of drop number $N(D)$ and liquid water $S_M(D)$ versus drop diameter for the events shown in Figs. 3–6. The dashed curves in Fig. 8 show the number density spectra that would have been obtained if the raw reflectivity data had been used to calculate the corresponding number densities. It is seen that the modification due to clear-air turbulence is very substantial and can change the results by an order of magnitude.

Figure 9 shows the result for liquid water density. Here the uncorrected spectrum is shown only for gate 18 to avoid cluttering the plot, but it is clear that correction for turbulence again can cause order-of-magnitude changes especially at the larger drop sizes.

Apparently turbulence has a very strong influence on the radar-deduced size distributions of both number density and liquid water. For very small droplets, the water particles act much like passive tracers of the air motion, and the radar backscatter spectra then simply provide the usual "clear-air" Doppler information about the turbulent velocity distribution. This is the

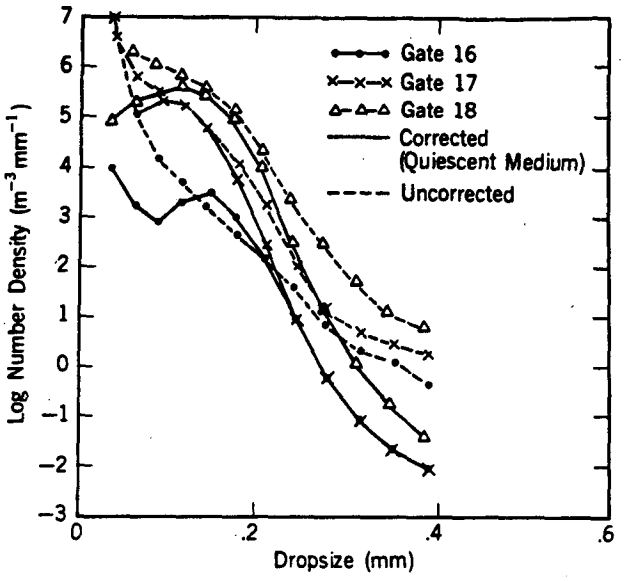

FIG. 8. Number density spectra for gates 16, 17 and 18 proceeding from edge of virga into its interior. Solid curves are spectra corrected for turbulence; dashed curves are corresponding uncorrected spectra shown for comparison.

basis of our suggestion that the spectral slope of the small droplet side of the droplet peak may provide a useful estimate of turbulence when the clear-air return is obscured. However, there must be a small-size limit for which the technique developed in this paper is useful, and therefore the observed spectrum for gate 18 (the dashed curve of Fig. 9) is compared with the result that would have been observed by the radar if there had been only a single drop-size population with quiet-air fall velocity $W = 1$ m s^{-1}, simply smeared by the turbulence (see Fig. 2). Assuming $W_\sigma = 0.3$, as was done in analyzing the gate 18 observational results, we find the dotted curve. It is substantially different from the dashed curve, supporting the contention that the observed radar spectra contain important information about the real drop-size distributions of number density and liquid.

Aside from possible uncertainties in calibration and data acquisition, we believe the primary errors in the method relate to uncertainty in the estimate of W_σ. The estimates of W_σ from the spectra used in this paper ranged from 0.3 to 0.4 m s^{-1}. Therefore in Fig. 9 the liquid water distribution for gate 18 was calculated for $W_\sigma = 0.4$ (dash–dot curve) for comparison with $W_\sigma = 0.3$ (solid curve). Comparison of the dash–dot curve with the solid curve (gate 18) provides an estimate of uncertainty in the liquid water distribution associated with uncertainty in the clear-air Doppler spectrum.

6. Implications for hydrometeor research

For the radar used in this study, the clear-air and cloud returns are usually smeared together and their separation is ambiguous. Only occasionally are cloud types observed for which the spectral separation is clear as in Fig. 1. Our immediate identification of the portion of our spectra due to clouds and that due to clear air rests on separation of spectral peaks with different vertical velocities. Equation (2) shows that the Rayleigh return from spherical water drops is proportional to λ^{-4}, whereas the clear-air return is proportional to $\lambda^{-1/3}$. Therefore long wavelength radars ($\sim$6 m) can unambiguously separate the clear-air spectrum from the spectrum of the very large drops such radars sense. On the other hand, short wavelength radars, such as those of 8 mm wavelength typically used in cloud studies, sense even nonprecipitating particles effectively. Near cloud boundaries the "clear-air" backscatter is sometimes enhanced by as much as an order of magnitude (Gossard and Strauch 1981), so there may be some risk of "clear-air" scatter contributing to the cloud return even at such a short wavelength, and it may not be feasible to cross-calibrate a 6 m wavelength radar and an 8 mm radar accurately enough to sort out the clear-air contribution. Fall velocities (relative to the mean air motion) of less than about 0.5 m s^{-1} would probably never be useful, because fall velocity is the fundamental quantity that provides the drop-size information sought. Therefore, the primary function of the long wavelength radar would be to provide the mean vertical air motion and the magnitude of the turbulent broadening of the spectrum. There are im-

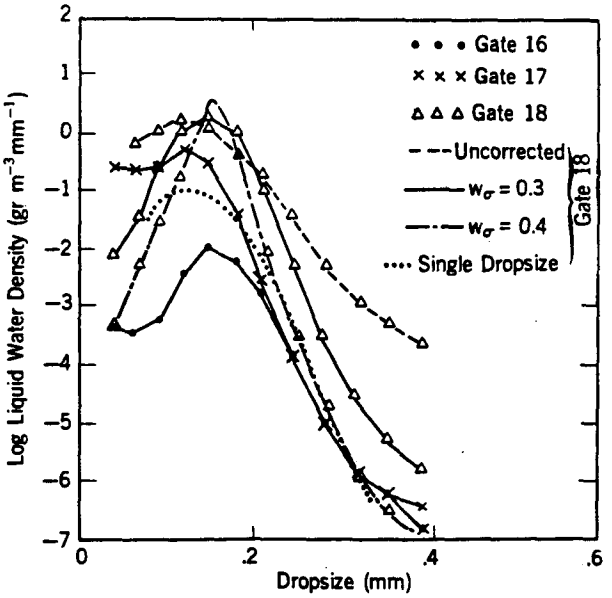

FIG. 9. Liquid water density spectra corresponding to the corrected number density spectra shown in Fig. 8. Only the uncorrected spectrum for gate 18 is shown (dashed). The dotted curve shows the theoretical spectrum that would be sensed by radar if a single drop-size medium (with a terminal velocity of 1 m s^{-1}) were perturbed by a Gaussian turbulence for which $W_\sigma = 0.3$. It should be compared with the spectra (e.g., the dashed curve) actually measured.

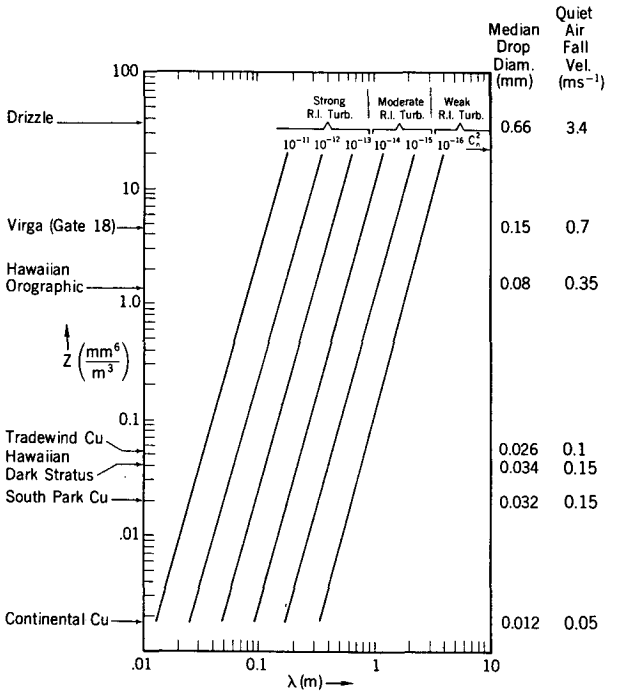

FIG. 10. Radar wavelength $\lambda(m)$ for which the Bragg return from clear air is equal to the return from clouds of Rayleigh droplets. Various cloud types are indicated along the left (Z) scale, and their corresponding median diameters and fall velocities (from Mason (1971)) are shown along the right margin of the figure.

portant constraints on the design of such a system—especially the antenna of the longer wavelength radar—because of the desirability of a narrow beam to minimize artificial spectral broadening. Several factors other than turbulence can broaden the measured Doppler spectrum such as wind shear, antenna motion, and beamwidth. For a vertically pointing antenna, vertical shear of the horizontal wind is negligible except under special conditions when the mean flow streamlines are not horizontal (as in a lee wave, for example). Therefore, if the vertically pointing antenna is stationary, our main concern is the width of the antenna beam. If the width of the antenna is substantial, a horizontal wind blowing across the vertically pointing beam produces a velocity component toward the radar at the leading edge of the beam and away from the radar at the trailing edge. For a Gaussian shaped beam, this contribution to the beam broadening is (Sloss and Atlas 1968)

$$W_{\sigma_A}^2 = V_T^2\theta^2/2.76 \qquad (13)$$

where θ is the one-way halfwidth to the half power (3 dB) point on the (Gaussian) antenna pattern in radians, and V_T is the wind component transverse to the beam axis. For the beamwidth of the antenna used in this paper (see Table 1) the broadening effect of (13) is small compared with the uncertainties in judging W_σ from noisy spectra for reasonable horizontal winds. However, for VHF radars with beamwidths typically from 3.6° to 7° this correction can be relatively large in percent (for moderate horizontal winds) if the turbulence is fairly weak as might be expected in stratiform clouds. Therefore, the antennas required for the longer wavelengths must be large and pose a financial problem for research facilities or for multiple radar networks.

The use of a single wavelength radar system is very attractive because of the imminent availability of a network of "clear-air" wind profilers. For such a system, separation of the cloud return from the clear-air return depends on identification of separate peaks in the spectrum, as in the cases used in this paper. Such identification depends on substantial vertical velocity of the droplets relative to the clear air, and on the two contributions being of comparable magnitude. From a forward scatter experiment in which the common volume of the transmitting and receiving radars was chosen to be inside fairly uniform nonprecipitating summer clouds in Colorado, Gossard and Strauch (1981) found (from horizontal beam swinging) that the "cross-over" in importance of cloud scatter and clear-air scatter occurred at wavelengths of 20–30 cm; for shorter wavelengths cloud particulate return was dominant and for longer wavelengths Bragg scatter was dominant. This wavelength range is close to the wavelength (32 cm) of the radar that acquired the data in

TABLE 2. Radar reflectivity factor for which cloud and clear returns are equal for 915 MHz radar.

Cloud type	Z (mm⁶ m⁻³)	C_n^2 10^{-14}	C_n^2 10^{-15}	C_n^2 10^{-16}	Diameter (mm)	Term. fall (m s⁻¹) velocity eq. (10)
Continental cumulus	1.82×10^{-3}	0.089	0.16	0.30	0.012	0.05
South Park cumulus	1.79×10^{-2}	0.16	0.30	0.57	0.032	0.15
Hawaiian dark stratus	$.4 \times 10^{-2}$	0.20	0.38	0.71	0.034	0.15
Tradewind cumulus	5.3×10^{-2}	0.22	0.40	0.76	0.026	0.1
Hawaiian orographic	1.35	0.53	0.99	1.85	0.08	0.35
Virga (gate 18)	4.5	0.75	1.41	2.64	0.15	0.7
Drizzle	37.7	1.31	2.45	4.59	0.66	3.4
Light rain	307	2.32	4.34	8.14	0.90	4.3

this paper, and the frequent separation of the two peaks supports the cross-over range found by Gossard and Strauch. For the substantial fall velocities seen in the virga of Fig. 6, the droplet peak in the heart of the virga dominates the Bragg return, as expected; it is, in fact, at least an order of magnitude greater. Therefore, if our interest lies in cloud particles having about 1 m s^{-1} fall velocity and greater, a longer radar wavelength would have provided a better balance between the two types of return. In order for the radar reflectivity from Rayleigh water droplets to be equal to Bragg backscatter from the clear-air equality of the right-hand members of (2) and (3) is required; i.e.,

$$Z\,(\mathrm{mm}^6\,\mathrm{m}^{-3}) = 1.335 \times 10^{15}\lambda^{11/3}C_n^2 \quad (14)$$

where C_n^2 is the refractive index structure parameter characterizing the turbulent fluctuations in refractive index. This relationship is shown plotted in Fig. 10. Typical values of C_n^2 lie between 10^{-14} and 10^{-15}. The figure includes data on cloud types summarized from Tables 4-1, 4-3, and 4-4 of Gossard and Strauch (1983) compiled from many sources. From the indicated median fall velocities it seems likely that the determination of drop-size distributions by the methods of this report will be useful for those cloud types between tradewind cumulus and drizzle using the 74 cm wavelength radars of the NWS profiler network.

If the peaks in the spectrum are not adequately separated, it is suggested that the clear-air and drop-size spectrum information be obtained from the heavy-lined portions of the spectrum shown schematically in Fig. 11.

7. Conclusions

It is possible to use modern clear-air radar technology to construct a remote sensing hydrometeor spectrometer, or disdrometer, useful over a band of drop sizes extending from the largest water drops down to droplets of about 100 μm diameter.

For some purposes a two wavelength radar system may be useful—one radar with a wavelength of several meters and another with a wavelength of about 8 mm. However, such a system poses design problems and would be expensive. Therefore, it would be desirable to use the NWS network of clear-air wind profilers for limited ranges of drop size and velocity for which their wavelength is suitable. An analysis of the available data on drop sizes of cloud types suggests that the 405 MHz radar network may be particularly useful for studies of liquid virga, Hawaiian orographic clouds and clouds producing light drizzle.

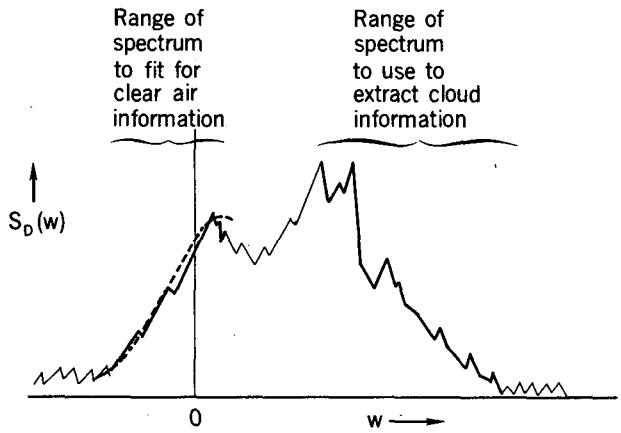

FIG. 11. Schematic description of a suggested procedure for getting a best fit of the clear-air velocity distribution and a best estimate of the drop-size distribution from a single wavelength Doppler radar.

Acknowledgments. The author wishes to express his appreciation to Richard Strauch for providing the data used in this paper, and to Nandini Sengupta and Bruce Sweezy for use of their data analysis, processing and to both Bob Weber and Richard Strauch for important suggestions improving the manuscript's content and presentation. Special thanks are also due Martin Decker for advice and for data collected by the radiometer.

REFERENCES

Atlas, D., 1964: Advances in radar meteorology. *Advances in Geophysics,* Academic Press, **10,** 318–478.

——, R. C. Srivastava and R. S. Sekon, 1973: Doppler radar characteristics of precipitation at vertical incidence. *Rev. Geophys. Space Phys.,* **11,** 1–35.

Batchelor, G. K., 1959: *Theory of Homogeneous Turbulence.* Cambridge University Press, 169 pp.

Beard, K. V., and H. R. Pruppacher, 1969: The determination of the terminal velocity and drag of small water drops by means of a wind tunnel. *J. Atmos. Sci.,* **26,** 1066–1072.

Battan, L. J., 1973: *Radar Observation of the Atmosphere.* The University of Chicago Press, 323 pp.

Boyenval, E. H., 1960: Echoes from precipitation using pulsed Doppler radar. *Proc. Eighth Weather Radar Conf.,* San Francisco, Amer. Meteor. Soc., 57–64.

Caton, P. G. F., 1963: The measurement of wind and convergence by Doppler radar. *Proc. Tenth Weather Radar Conf.,* Washington, DC, Amer. Meteor. Soc., 290–296.

——, 1966: Raindrop-size distributions in the free atmosphere. *Quart. J. Roy. Meteor. Soc.,* **92,** 15–30.

Doviak, R. J., and D. S. Zrnić, 1984: *Doppler Radar and Weather Observations.* Academic Press, 458 pp.

du Toit, P. S., 1967: Doppler radar observations of drop sizes in continuous rain. *J. Appl. Meteor.,* **6,** 1082–1087.

Foote, G. B., and P. S. du Toit, 1969: Terminal velocity of raindrops aloft. *J. Appl. Meteor.,* **8,** 249–253.

Gorelik, A. G., I. V. Gritskiv, L. A. Penyax and V. V. Tsykunov, 1967: Results of simultaneous radar and ground measurements of the microstructure of precipitation. *Izv. Akad. Nauk SSSR, Ser. Fiz. Atmos. Okeana,* **3,** 961–966.

Gossard, E. E., and R. G. Strauch, 1981: The refractive index spectra within clouds from forward-scatter radar observations. *J. Appl. Meteor.,* **20,** 170–183.

——, and ——, 1983: *Radar Observations of Clear Air and Clouds.* Elsevier, 280 pp.

Green, J. L., R. H. Winkler, J. M. Warnock, W. L. Clark, K. S. Gage and T. E. VanZandt, 1978: Observations of enhanced clear-air reflectivity associated with convective clouds. *18th Conf. on Radar Meteorology,* Atlanta, Amer. Meteor. Soc.

Gunn, R., and G. D. Kinzer, 1949: The terminal velocity of fall for water droplets in stagnant air. *J. Meteor.,* **6,** 243–248.

Labbitt, M., 1981: Coordinated radar and aircraft observations of turbulence. Lincoln Lab. Rep. ATC-108, 39 pp.

Lhermitte, R., 1960: The use of special "pulsed Doppler radar" in measurements of particle fall velocities. *Proc. Eighth Weather Radar Conf.*, San Francisco, Amer. Meteor. Soc., 269–275.

Lumley, J. L., and H. A. Panofsky, 1964: *Structure of Atmospheric Turbulence.* Interscience Publishers, 94 pp.

Mason, B. J., 1971: *The Physics of Clouds.* Clarendon Press, Oxford, 659 pp.

Rogers, R. R., and R. J. Pilié, 1962: Radar measurements of drop size distribution. *J. Atmos. Sci.*, **19,** 503–506.

Sengupta, N., J. M. Warnock, E. E. Gossard and R. G. Strauch, 1987: Remote sensing of meteorological parameters with the aid of a clear-air Doppler radar. NOAA TM ERL 431-WPL61.

Sloss, D. H., and D. Atlas, 1968: Wind shear and reflectivity gradient effects on Doppler radar spectra. *Preprints, 13th Radar Meteorology Conf.*, Montreal, Amer. Meteor. Soc., 44–49.

Strauch, R. G., D. A. Merritt, K. P. Moran, K. B. Earnshaw and D. van de Kamp, 1984: The Colorado wind-profiling network. *J. Atmos. Oceanic Technol.*, **1,** 37–49.

Tennekes, H., and J. L. Lumley, 1972: *A First Course in Turbulence.* M.I.T. Press, 246 pp.

Ugai, S., K. Kato, M. Nishijima and T. Kan, 1977: Characteristics of raindrop size and raindrop shape. *Comptes Rendus Proc.*, URST Comm. F, La Baule, France.

Wakasugi, K., A. Mizutani, M. Matsuo, S. Fukao and S. Kato, 1986: A direct method for deriving drop-size distribution and vertical air velocities from VHF Doppler radar spectra. *J. Atmos. Oceanic Technol.*, **3,** 623–629.

——, ——, ——, —— and ——, 1987: Further discussion on deriving drop-size distribution and vertical air velocities directly from VHF Doppler radar spectra. *J. Atmos. Oceanic Technol.*, **4,** 170–179.

Wilson, D. A., 1963: Drop size distribution as recorded by pulsed Doppler radar. Master's thesis, University of Arizona, 64 pp.